








Article

Effect of Deposition Temperature and Thermal Annealing on the Properties of Sputtered NiO_x/Si Heterojunction Photodiodes

Roumen Nedev¹, David Mateos-Anzaldo^{1,*}, Eddue Osuna-Escalante¹, Oscar Perez-Landeros¹,
Mario Curiel-Alvarez¹, Esteban Osorio-Urquizo¹, Jhonathan Castillo-Saenz¹, Javier Lopez-Medina²,
Benjamin Valdez-Salas¹ and Nicola Nedev^{1,*}

¹ Instituto de Ingeniería, Universidad Autónoma de Baja California, Blvd. Benito Juárez s/n, Mexicali C.P. 21280, Mexico; roumen.nedev@uabc.edu.mx (R.N.); eddue.osuna@uabc.edu.mx (E.O.-E.); operez55@uabc.edu.mx (O.P.-L.); mcuriel@uabc.edu.mx (M.C.-A.); esteban.osorio@uabc.edu.mx (E.O.-U.); jhonathan.saenz@uabc.edu.mx (J.C.-S.); berval@uabc.edu.mx (B.V.-S.)

² Conahcyt Centro de Nanociencias y Nanotecnología, Universidad Nacional Autónoma de México, Ensenada C.P. 22800, Mexico; javierlo21@ens.cnyn.unam.mx

* Correspondence: dmateos@uabc.edu.mx (D.M.-A.); nicolan@uabc.edu.mx (N.N.)

Abstract: NiO_x is a p-type semiconductor with excellent stability, which makes it interesting for a wide range of applications. Broadband photodetectors with high responsivity (*R*) were fabricated by depositing r.f.-sputtered NiO_x layers on n-Si at room temperature (RT), 50 °C and 100 °C. In self-powered mode the RT diodes have *R* between 0.95 and 0.39 A/W for wavelengths between 365 and 635 nm, while at a reverse bias of −4 V, the responsivity increases to values between 22 A/W and 10.7 A/W for wavelengths in the same range. The increase of the deposition temperature leads to a decrease of *R* but also to a smaller reverse dark current. Thus, the 100 °C photodiodes might be more appropriate for applications where high responsivity is required, because of their smaller power consumption compared to the RT diodes. In addition, it was found that the increase of the deposition temperature leads to an increase of the diodes' series resistance and the resistivity of NiO_x. The effect of Rapid Thermal Annealing (RTA) on the properties of the photodiodes was studied. Annealing at 550 °C for 6 min leads to much higher responsivity compared to *R* of diodes with as-deposited NiO_x. However, a disadvantage of the annealed diode is that the reverse current depends on the amplitude and polarity of previously applied bias voltage. The higher responsivity of the RTA photodiodes makes them useful as light sensors.

Keywords: NiO_x-nSi broadband photodetectors; high responsivity; r.f. sputtering; effect of RTA treatment; light sensors



Academic Editors: Sake Wang, Minglei Sun and Nguyen Tuan Hung

Received: 30 November 2024

Revised: 29 December 2024

Accepted: 30 December 2024

Published: 3 January 2025

Citation: Nedev, R.; Mateos-Anzaldo, D.; Osuna-Escalante, E.; Perez-Landeros, O.; Curiel-Alvarez, M.; Osorio-Urquizo, E.; Castillo-Saenz, J.; Lopez-Medina, J.; Valdez-Salas, B.; Nedev, N. Effect of Deposition Temperature and Thermal Annealing on the Properties of Sputtered NiO_x/Si Heterojunction Photodiodes. *Inorganics* **2025**, *13*, 11. <https://doi.org/10.3390/inorganics13010011>

Copyright: © 2025 by the authors. Licensee MDPI, Basel, Switzerland. This article is an open access article distributed under the terms and conditions of the Creative Commons Attribution (CC BY) license (<https://creativecommons.org/licenses/by/4.0/>).

1. Introduction

NiO_x is a p-type semiconductor with excellent chemical stability and high transmittance in the visible part of the electromagnetic spectrum [1]. Its bandgap varies between 3.4 and 4.3 eV depending on the deposition technique and conditions. Due to its electrical and optical properties, NiO_x is considered an attractive material for various applications, such as photovoltaic devices [2], electrochromic devices [3], gas sensors [4] and ultraviolet and broadband photodetectors [5–8]. Various physical and chemical deposition techniques have been used to prepare NiO_x films. Among the most commonly used methods are sputtering [9], sol–gel spin-coating [10–12], electron beam evaporation [7] and chemical vapor deposition [13]. The structural, optical and electrical properties of the NiO_x layers depend strongly on the deposition technique [14–16]. The magnetron r.f. sputtering is

widely used because of the following advantages: high film quality, low density of defects, high adhesion, low cost and high deposition rate. NiO_x films have been deposited by d.c. and r.f. sputtering. Metallic Ni in an Ar/O₂ gas atmosphere has been used in the d.c. sputtering process. The r.f. sputtering of an NiO target has been carried out in Ar/O₂ and pure Ar atmospheres [14,17–21]. Despite recent advances, some challenges remain regarding the optimization of the optical and electrical properties of r.f.-sputtered NiO_x layers, especially for application in photodetectors. Variations of process parameters, such as substrate temperature, deposition power, base and working pressures, affect the deposited film characteristics.

Wang et al. reported the effect of varying the deposition temperature during reactive sputtering with a fixed r.f. power of 110 W [17]. Jamal et al. studied the effect of the variation of the growth temperature in the range between room temperature (RT) and 400 °C on the properties of r.f.-sputtered NiO thin films, demonstrating that increasing the substrate temperature to 100 °C results in suitable properties for photovoltaic applications [18]. Ahmed et al. reported the effect of r.f. power used in the deposition and showed that the best structural, morphological and optical properties of NiO were obtained at sputtering power of 200 W [19]. Elmassi et al. investigated the variation of r.f. power on structural properties of NiO thin films obtained in an O₂/Ar atmosphere, finding a relationship between power increment and crystallite size [20]. Abdur et al. investigated the impact of open-air post-annealing on the optoelectrical and structural properties of NiO films, reporting that films deposited at 100 °C showed favorable crystalline quality with the highest observed carrier mobility [21].

However, the results for the effect of the deposition temperature and thermal annealing processes on the properties of broadband photodetectors are limited. In this work, we study the properties of NiO_x layers deposited by r.f sputtering from an NiO target at a fixed r.f. power of 60 W and temperatures between RT and 100 °C. In addition, the effect of post-deposition annealing of NiO_x films on the optical and electrical properties of the metal/NiO_x/nSi heterojunction diodes was studied.

2. Results

Figure 1a shows the experimental dependencies of the ellipsometric parameters Ψ and Δ , and the fitted curves using the Cauchy dispersion model for an NiO_x layer deposited at 100 °C and subjected to Rapid Thermal Annealing (RTA). Similar fitting results were obtained for the as-deposited layers prepared at RT, 50 °C and 100 °C, and for the RTA layers deposited at the other two temperatures, RT and 50 °C. Figure 1b,c show the refractive index of the as-deposited and annealed NiO_x films. From results in Figure 1b,c, it may be concluded that the RTA process does not lead to an important change of the optical constants. The layer thicknesses, deposition rate, the refractive index (n) and the extinction coefficient (k) at 632.8 nm of the as-deposited layers are shown in Table 1. The smaller thickness of the films deposited at 100 °C may be explained by assuming that during the deposition process at 100 °C, the substrate provides sufficient thermal energy to weakly bonded atoms to leave the surface. The obtained values for the optical constants n and k are close to ones reported in the literature for NiO_x [19].

Figure 2a shows transmission spectra of a corning glass (CG) substrate and CG coated with NiO_x layers deposited at RT, 50 °C and 100 °C. The transparency of CG was $\geq 80\%$ in the range of 350–1000 nm. The transmittance of the samples with an NiO_x layer varies between ~60 and 80% in the visible—near IR range (400–1000 nm). Using the Tauc plot method, the band gaps E_g of the films were obtained for the three deposition temperatures, 3.79, 3.82 and 3.91 eV, respectively (Figure 2b). These results are in agreement with previously published values for E_g of NiO [7,22–24].

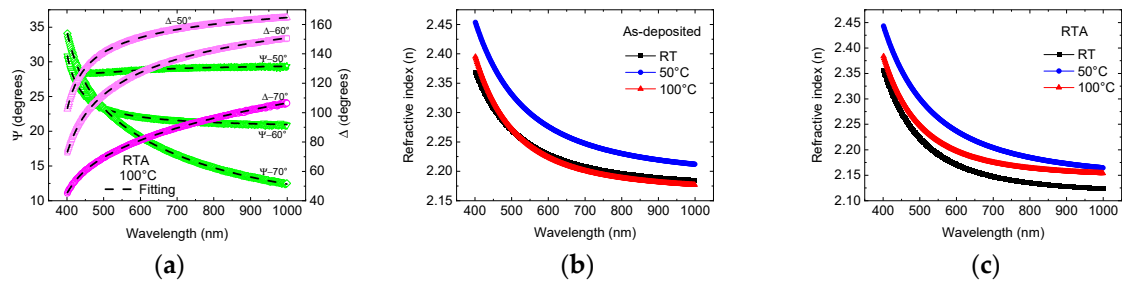


Figure 1. (a) Experimental Ψ and Δ dependences and the fitted curves for a layer deposited at 100 °C and subjected to RTA. Refractive index for: (b) As-deposited layers; (c) RTA annealed layers.

Table 1. Thickness, deposition rate and optical constants n and k at 632.8 nm for layers deposited at the three temperatures.

Temperature (°C)	Thickness (nm)	Deposition Rate (nm/min)	n	k
RT	41.5	6.9	2.25	0.03
50	48.9	8.2	2.29	0.044
100	36.0	6.0	2.25	0.01

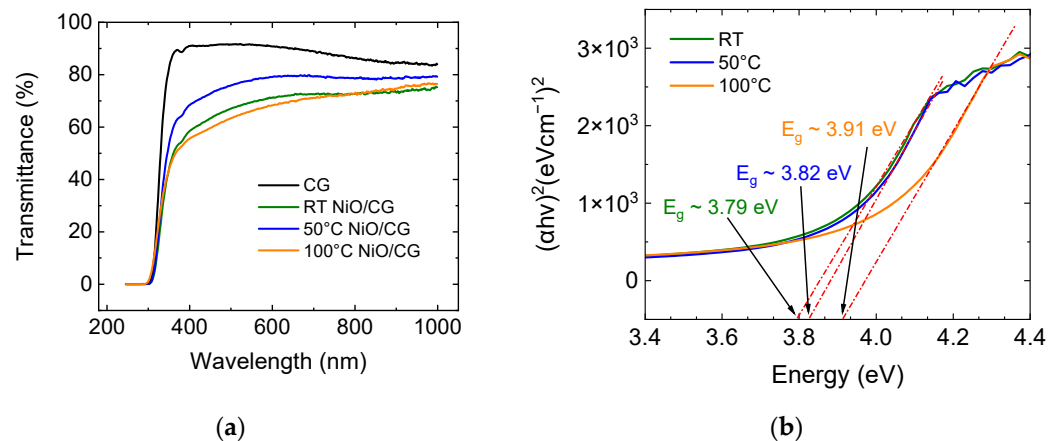


Figure 2. (a) Transmittance of CG substrate and CG coated with NiO_x layers deposited at RT, 50 °C and 100 °C; (b) band gaps of the films determined by the Tauc plot method.

Atomic force microscopy (AFM) was used to characterize the surface morphology of as-deposited and annealed layers on an Si substrate (Figure 3). Smooth surfaces were obtained for films deposited at RT, 50 °C and 100 °C with root mean square (RMS) values of 0.6, 0.49 and 0.46 nm, respectively. The slight decrease of RMS with the temperature may be explained by assuming that the thermal energy provided by the substrate leads to some rearrangement of the surface atoms, which results in smoother surface. After the RTA, the values of RMS for layers deposited at RT, 50 °C and 100 °C are 0.72, 0.42 and 0.62 nm. Interestingly, the annealing process leads to a slight increase of the roughness of the RT and 100 °C films, but to a small decrease of RMS of the 50 °C layer.

A schematic diagram of the structure of the studied photodiodes and the experimental setup used in the electrical characterization is shown in Figure 4. The applied bias was defined relative to the back contact of the Si substrate; therefore, reverse bias means negative voltage applied on the top metal electrode.

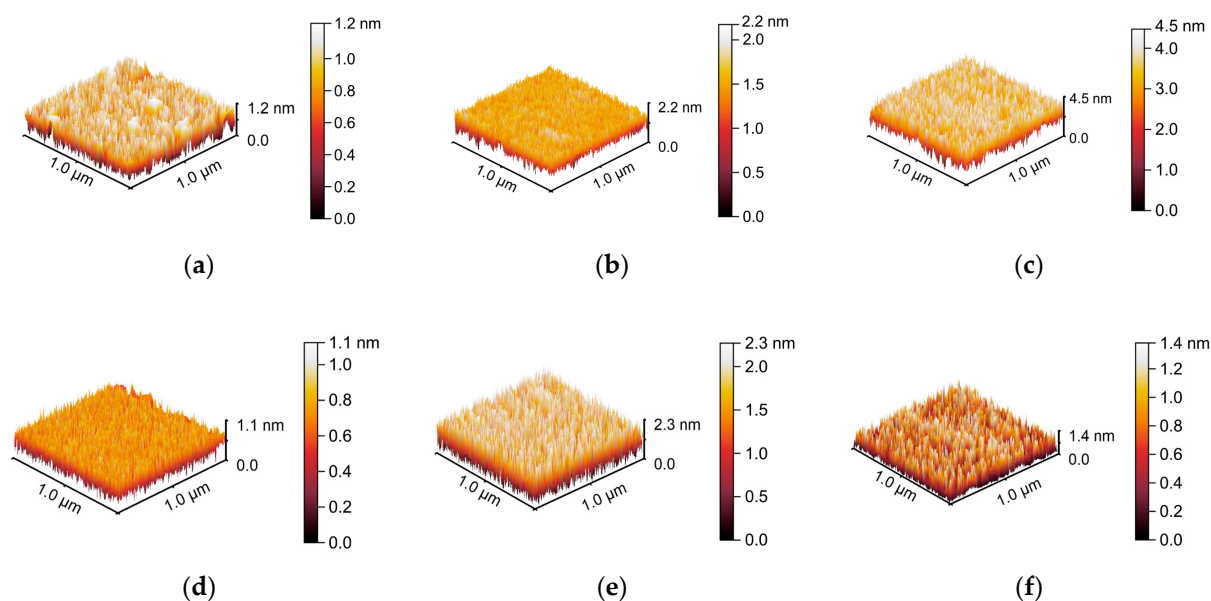


Figure 3. AFM results of as-deposited NiO_x layers obtained at: (a) RT, (b) 50 °C and (c) 100 °C and of RTA annealed layers deposited at: (d) RT, (e) 50 °C and (f) 100 °C.

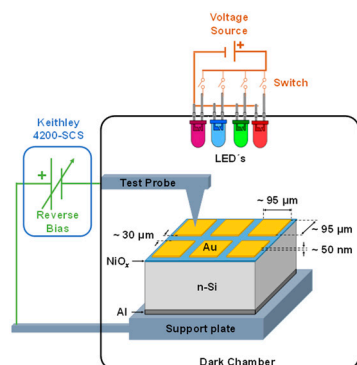


Figure 4. Schematic diagram of the structure of the studied devices with definition of the bias voltage polarity.

Current–voltage (I - V) characteristics of photodiodes with NiO_x layers deposited at RT, 50 °C and 100 °C were measured by ramping the bias voltage in both directions (Figure 5). No hysteresis was observed in these measurements as well as after various consecutive measurements, indicating low density of deep traps in the NiO_x layer and in the NiO_x/Si interfacial region. Typical rectifying dependences were measured with reverse saturation dark currents of $\sim 3 \times 10^{-7}$, 7×10^{-7} and 1×10^{-7} A for the three deposition temperatures. Under forward bias, the current increases exponentially to voltages of ~ 1 V for the RT diode and to ~ 0.7 V for the other two diodes, and then the characteristics change their shape because of the diodes' series resistance. All diodes show photoresponses under reverse bias voltages ($V_r < 0$ V) and in self-powered mode ($V = 0$ V). The short-circuit currents (I_{SC}) under illumination with red, green, blue and UV light for the diodes with NiO_x deposited at the three temperatures are given in Table 2. The open-circuit voltage (V_{OC}) depends slightly on the light intensity and varies between 0.2 V and 0.35 V depending on the light intensity and the NiO_x deposition temperature (Figure 5a–c). The photoresponses of the diodes with the NiO_x layer deposited at 100 °C are higher than those of the diodes obtained at 50 °C and are close to those of the diodes obtained at room temperature. However, an advantage of the 100 °C photodiodes is their smaller reverse dark current compared to the RT diodes.

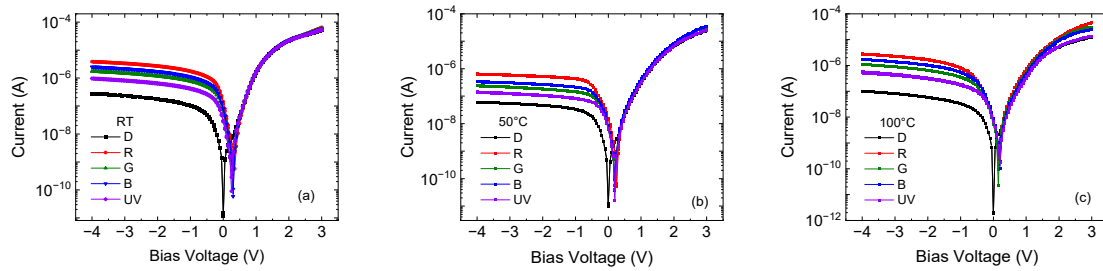


Figure 5. *I-V* characteristics of photodiodes with NiO_x layers deposited at: (a) RT, (b) 50 °C and (c) 100 °C measured in the dark and under illumination with red, green, blue and UV light.

Table 2. Short-circuit currents under illumination with red, green, blue and UV light for the diodes with NiO_x deposited at the three temperatures.

Light Color	<i>I_{SC}</i> (A)		
	RT	50 °C	100 °C
Red	1.30×10^{-7}	1.50×10^{-8}	7.85×10^{-9}
Green	5.70×10^{-8}	6.70×10^{-9}	9.15×10^{-9}
Blue	7.97×10^{-8}	8.50×10^{-9}	5.25×10^{-9}
UV	2.87×10^{-8}	6.40×10^{-9}	6.85×10^{-9}

Figure 6 shows a schematic band diagram of a p-NiO_x/n-Si photodiode under short-circuit conditions. Under illumination with each of the four light-emitting diodes (LEDs) used in this study, the light passes through the NiO_x layer since the photons' energy is smaller than the NiO_x bandgap. Then, the photons are absorbed in Si, generating electron-hole pairs. The pairs generated in the depletion region and within a hole diffusion length from the transition region are separated by the internal electric field, resulting in *I_{sc}* flowing through the diode. At reverse bias, the space charge region and the electric field at the heterojunction increase, leading to an increase of the photocurrent (Figure 5).

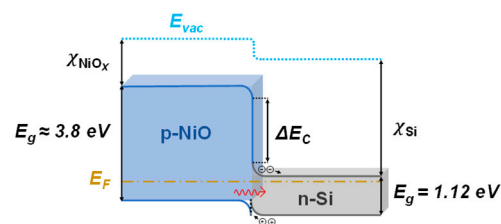


Figure 6. Schematic energy band diagram of a p-NiO_x/n-Si diode under short-circuit conditions, $V = 0$ V.

I-V characteristics of diodes with NiO_x layers deposited at the three temperatures and subjected to the RTA process are shown in Figure 7. The thermal annealing leads to several important changes in the *I-V* dependences. Thus, the dark current and the photocurrents depend on the direction in which the bias voltage changes, leading to hysteresis at both the forward and reverse bias ramps. For forward biases, the current measured with bias increasing from 0 V towards positive voltages is smaller than the current measured in the opposite direction, most clearly seen in Figure 7b. The hysteresis is more pronounced under reverse biases and increases with the NiO_x deposition temperature. The reverse bias voltages at which the current reaches saturation are close to or greater than -10 V (Figure 7a–c). The photocurrents at these large negative voltages are greater than the photocurrents of the diodes with as-deposited NiO_x layers. The highest values were obtained for the 50 °C, RTA diode (Figure 7b). However, the *I-V* hysteresis of the annealed

photodiodes can be a disadvantage in their practical application. The inset in Figure 7b shows a zoomed view of the current in the region of -0.5 – 0.5 V of a characteristic that was measured between 5 V and -10 V and then in the opposite direction. It can be seen that when ramping the bias from positive voltages towards 0 V, the characteristic crosses the x -axis at a positive voltage of 0.3 V, indicating increase of the negative charge trapped in the structure. In contrast, when the bias voltage varies from -10 V towards 0 V, the characteristic crosses the x -axis at -0.3 V, indicating increase of the positive trapped charge. Therefore, the observed hysteresis is more likely due to change of the charge state of shallow traps at the $\text{NiO}_x/\text{n-Si}$ heterojunction interface and in the interfacial region with the bias voltage. As a result, no open-circuit voltage and short-circuit current were measured. Since no shift was observed of the I - V curves of diodes with as-deposited NiO_x layers, it may be concluded that the RTA process has created defects, which can exchange carriers with Si, and as a result change their charge state.

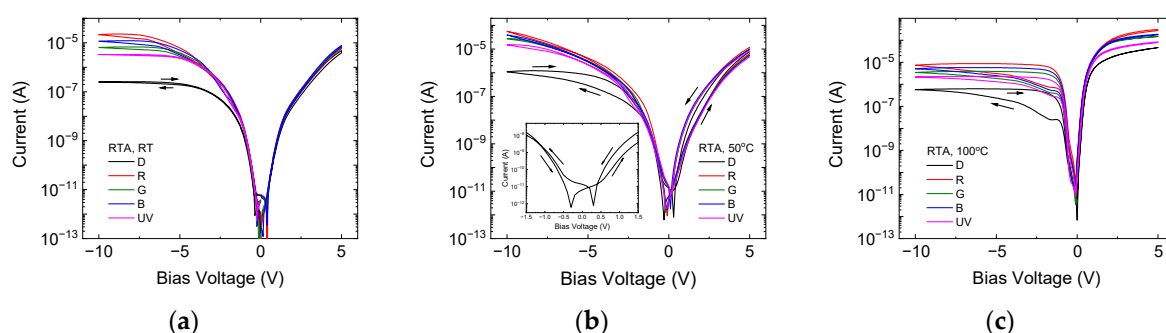


Figure 7. I - V characteristics of photodiodes with NiO_x layers deposited at: (a) RT, (b) 50°C and (c) 100°C and subjected to RTA annealing. The dependences were measured in the dark and under illumination with red, green, blue and UV light. The inset in (b) shows a zoomed view of the current in the region of -0.5 – 0.5 V of a characteristic measured between 5 V and -10 V and then in the opposite direction.

Capacitance–voltage (C - V) measurements were carried out in order to study in more detail the effect of consecutive bias voltage ramps on the charge state of the diodes. The results in Figure 8a show that ramping the voltage in both directions does not lead to hysteresis in the C - V curves of diodes with NiO_x layers deposited at the three temperatures, indicating that no charge was trapped during these measurements. In contrast, the C - V characteristics of the diodes subjected to RTA when measured under reverse bias sweep from 0 V to -10 V and back to 0 V show a displacement of the C - V curves, corresponding to increase of the trapped positive charge in the diodes (Figure 8b). In accordance with the I - V measurements, the diodes with NiO_x layers deposited at 50°C and 100°C show higher hysteresis in dark.

Time-dependent photoresponses of all photodiodes upon red, green, blue and UV light illumination was measured. The on/off switching curves (Figure 9) are characterized by the rise (τ_r) and fall (τ_f) times, defined as the time needed for the photocurrent to increase from 10% to 90% of its maximum value or to drop from 90 to 10%, respectively. The τ_r and τ_f values for the diodes with as-deposited layers are less than 0.1 s (Figure 9a–c). As could be expected from the I - V results obtained at reverse bias ramps, the RTA process can lead to an increase of the switching times. Thus, the τ_r values for the annealed samples deposited at RT, 50°C and 100°C are 9.5, 1.7 and 8.6 s, respectively. However, the τ_f times for the annealed diodes are <0.1 s. Another important observation is that at the voltage pulses used $V_r = -8$ V, the RTA diodes with an NiO_x layer deposited at 50°C reach faster saturation of the photocurrent (Figure 9e) compared to the other two diodes (Figure 9d,f). As it was mentioned above, the variation of the current at applied bias under light illumination could

be related to change of the charge state of shallow traps at the NiO_x/Si interface and in the interfacial region.

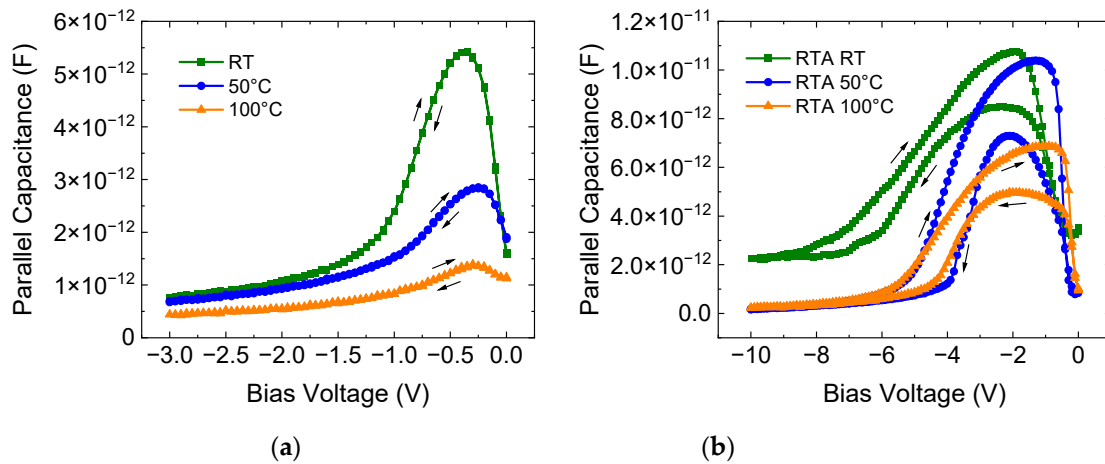


Figure 8. C-V characteristics measured in the dark under reverse bias of: (a) diodes with as-deposited NiO_x layers; (b) diodes with RTA annealed layers.

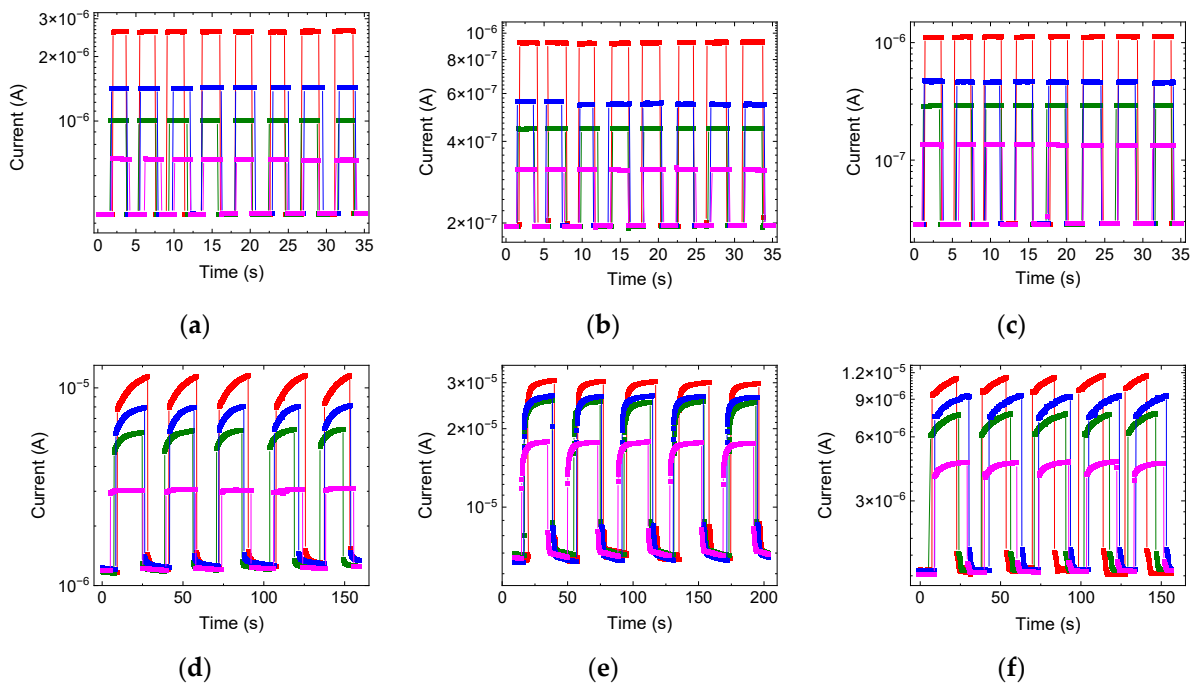


Figure 9. Time-dependent photoresponses of diodes with as-deposited NiO_x layers obtained at: (a) RT, (b) 50 °C, and (c) 100 °C, and of diodes with RTA annealed layers deposited at: (d) RT, (e) 50 °C, and (f) 100 °C. The switching curves of the diodes with as-deposited layers were measured at voltage pulses of -3 V, while the RTA diodes were measured at pulses of $V_r = -8$ V. The red, green, blue and violet color lines correspond to illumination with red, green, blue and UV LED, respectively.

3. Discussion

The series resistance (R_s) reduces the voltage applied on the heterojunction and, thus, affects the I - V characteristic. R_s can be evaluated from the slope of the I_f/g vs. I_f characteristic [25], where I_f is the forward current in the region after the exponential increase of I and g is the conductance dI_f/dV_f . In this region R_s leads to change of the shape of the I - V curve. The dependence of I/g on I may be derived by differentiating the I - V equation

$$I = I_0 \left(e^{\frac{q(V-IR_s)}{nkT}} - 1 \right),$$

where n is the ideality factor, which gives

$$\frac{dI}{dV} = I \frac{q}{nkT} \left(1 - R_s \frac{dI}{dV} \right),$$

or

$$g = I \frac{q}{nkT} (1 - R_s g),$$

By simple algebraic transformations, a linear dependence of I/g on the forward current I is obtained

$$\frac{I}{g} = \frac{nkT}{q} + R_s I$$

Figure 10a displays the I/g vs. I dependencies for no annealed diodes with NiO_x layers deposited at RT, 50 °C and 100 °C. The slope of the straight lines increases with the deposition temperature, indicating that R_s also increases. Since the resistivity of the n-type region of the heterojunction, n-Si, is constant, it may be concluded that the increase of the deposition temperature leads to an increase of the resistivity of the NiO_x layers. A similar effect of increased resistivity was observed at a constant deposition temperature with an increase of the r.f. power [26,27].

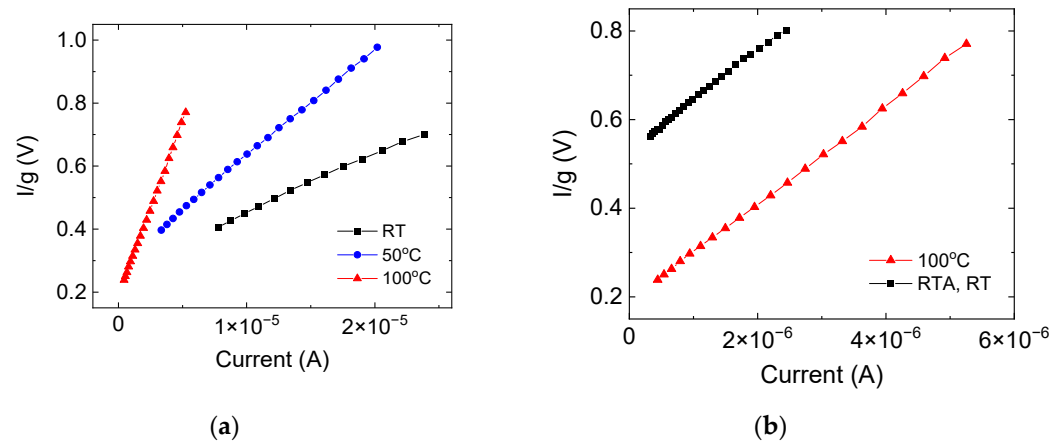


Figure 10. (a) I/g vs. I dependencies for diodes with as-deposited NiO_x layers prepared at RT, 50 °C and 100 °C. Higher line slope corresponds to higher R_s ; (b) comparison of the I/g vs. I dependencies for a diode with as-deposited NiO_x prepared at 100 °C (red line) and a RTA annealed diode with NiO_x layer deposited at RT (black line). Note the difference in x -axis scale.

The dependence of the forward current on the voltage sweep direction makes it impossible to evaluate the series resistances of the diodes after RTA. An approximate estimation was obtained for the RTA diode with an NiO_x layer deposited at RT (Figure 7a) by using the I - V characteristic measured from 0 V towards positive voltages. The obtained result is compared with the I/g vs. I dependence for a no annealed diode with an NiO_x layer deposited at 100 °C, the one with the highest R_s (Figure 10b). The line slopes in Figure 10b indicate that the RTA process leads to comparable or even higher values of R_s than those of the 100 °C diodes.

The responsivity (R) of the fabricated photodiodes was calculated from [28]

$$R = \frac{I_{ph}}{P_\lambda \cdot A}$$

where $I_{ph} = I_{light} - I_{dark}$ is the photocurrent, P_λ is the optical power intensity at a specific wavelength λ and A is the area of the top contact. Here, I_{light} and I_{dark} are the currents measured under light illumination and in dark conditions. High responsivity was determined

for the no annealed photodiodes. The results are shown in Figure 11a and in Table 3. The responsivity of the diodes with an NiO_x layer deposited at RT is higher than *R* of the other diodes in self-powered mode, as well as at reverse bias of −4 V. For applications where a self-biased mode of operation is required, the RT diodes are the most appropriate. However, for some applications where higher responsivity is required, the 100 °C photodiodes may be the better option because of their smaller dark current at −4 V and *R*, which is close to that of the RT diode. The responsivity of the diodes subjected to RTA under *V_r* = −10 V is shown in Figure 11b. Very high values for *R* were determined under bias voltage of −10 V, much higher than the ones reported in the literature for broadband photodetectors. While the *R* of the diode RTA annealed at 50 °C is the highest one, this diode can be less appropriate because of its higher dark current and lack of saturation of the photocurrent, even at reverse bias voltage of −10 V. Although the RTA annealed diodes may not be appropriate for applications where precise measurement of the optical power is required, they may be useful as light sensors because of their high responsivity.

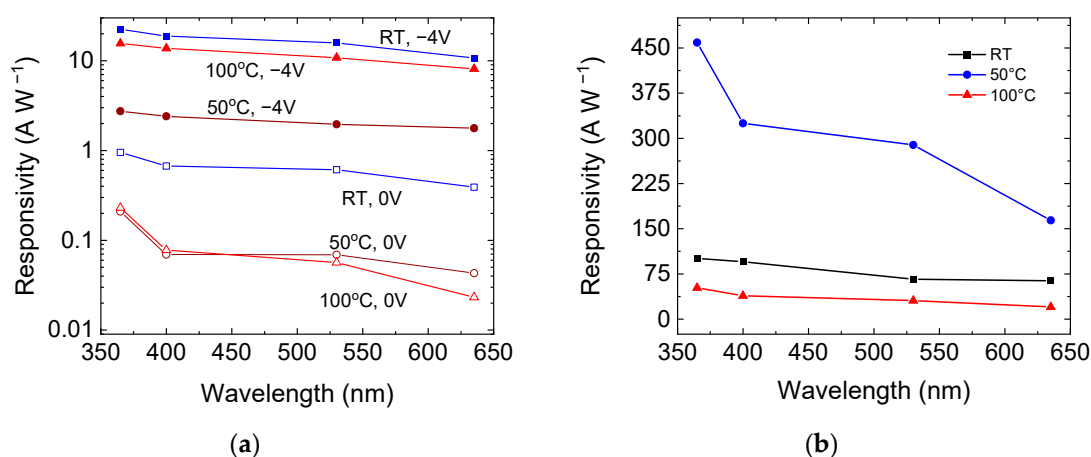


Figure 11. Responsivity of photodiodes with: (a) as-deposited NiO_x layers; (b) RTA annealed NiO_x layers.

Table 3. Responsivity of photodiodes with as-deposited NiO_x layers.

Wavelength (nm)	<i>R</i> (A/W), Self-Powered Mode			<i>R</i> (A/W), <i>V_r</i> = −4 V		
	RT	50 °C	100 °C	RT	50 °C	100 °C
635	0.39	0.045	0.023	10.7	1.77	8.1
530	0.61	0.072	0.056	15.8	1.96	10.8
400	0.67	0.072	0.077	18.8	2.4	13.7
365	0.95	0.21	0.23	22.4	2.74	15.6

The obtained results for *R* at 0 V and at −4 V for photodiodes with as-deposited NiO_x layers are compared with results reported in the literature in Table 4. The determined responsivity of the photodiodes deposited at RT and 100 °C are among the highest reported and are comparable with results published by other authors. Ma et. al. reported a responsivity of 15.8 A/W at −5 V, which is slightly higher than our result for 100 °C diodes, however the maximum bias voltage used here was −4 V.

Table 4. Comparison of NiO-based photodiode parameters reported in literature. P_{RF} stands for r.f. power.

Device	R (A/W)	D (Jones)	I_d (A)	On/Off Ratio	τ_r, τ_f (s)	Year [Ref.]
p-NiO/nSi	4.8×10^{-3} (at 318 nm)	-	-	-	-	2015 [29]
p-NiO/nSi	1.73, 1.81, 2.07 (at 5 V, 365, 625, 850 nm)	-	-	31, 35, 41 (at 5 V, 365, 625, 850 nm)	$3.49/7.68 \times 10^{-3}$	2022 [30]
NiO/TiO ₂	0.074 (at 0 V, 380 nm)	-	10^{-9}	922	$33.6/92.6 \times 10^{-3}$	2022 [31]
p-NiO/n-Si	0.95, 0.67, 0.61, 0.39 (at 0 V, 365, 400, 530, 635 nm, $P_{RF} = 60$ W) 22.4, 18.8, 15.8, 10.7 (at -4 V, 365, 400, 530, 635 nm)	5.5×10^{10} (at 0 V, 365 nm)	8.5×10^{-12} (at 0 V) 2.8×10^{-7} (at -4 V)	3.4×10^3 (at 0 V, 365 nm, $P_{RF} = 60$ W)	<0.1	2023 [27]
p-NiO/n-GaN	3.11×10^{-3} (at 0 V)	8.69×10^9	-	-	$2/47 \times 10^{-3}$	2024 [32]
NiO/Ga ₂ O ₃	5.08×10^{-3} (at -10 V, 254 nm)	3.19×10^{11}	2.76×10^{-12}	802.53	$62/67 \times 10^{-3}$	2024 [9]
NiO/Al ₂ O ₃ /n-Si	15.8 (at -5 V, 365 nm)	1.14×10^{14}	0.279×10^{-6}	-	$0.08/0.184 \times 10^{-3}$	2024 [33]
p-NiO/n-Si (100 °C)	15.6 (at -4 V, 365 nm) 0.23 (at 0 V, 365 nm)	8.41×10^{10} (at -4 V, 365 nm) 2.875×10^{11} (at 0 V, 365 nm)	1.02×10^{-7} 1.9×10^{-12}	68.23×10^{-3} 3.66×10^{-3}	<0.1 -	This work

Another relevant parameter is the specific detectivity (D^*), which can be defined as the sensibility of a photodiode to detect weak light signals. D^* involves the R at a given wavelength of the excitation light, the elementary charge (q) and the dark current density (J_D) and is given by

$$D^* = \frac{R_\lambda}{\sqrt{2qJ_D}}$$

The values obtained for the detectivity are close to the best values reported in the literature for NiO_x-based photodetectors (Table 4).

4. Materials and Methods

NiO_x thin films were deposited on n-type (100) Si wafers with resistivity of 4–10 Ω·cm by r.f. magnetron sputtering at 25 °C (RT), 50 °C and 100 °C. The deposition time was 6 min for the three temperatures. Prior to deposition, the substrates were cleaned in an ultrasonic bath for 5 min with acetone, isopropyl alcohol and deionized water and dried with high-purity nitrogen. NiO target (99.9%) with dimensions of 50.8 × 3.175 mm at a working distance of 7 cm was used for deposition. The sputtering gas was ultra-high-purity (UHP) argon (99.9999%). The chamber base pressure was 1×10^{-5} Torr, the working pressure was 5 mTorr and the Ar flow was 18.9 sccm. Before the deposition, the target was pre-sputtered for 20 min. To study the effect of thermal annealing, half of the samples were subjected to the RTA process in an UHP N₂ atmosphere. The annealing was performed in a horizontal tube furnace (Zhengzhou CY Scientific Instrument Co., Zhengzhou, China) equipped with a sliding rail. The samples were placed in a quartz tube under constant N₂ flow of 100 mL/min in a position outside of the furnace. The furnace was heated at a rate of 10 °C/min to the desired temperature and when it was reached, the furnace was moved to the position of the samples. The samples were annealed at 550 °C for 6 min. Following the annealing process, the furnace was returned to its initial position and the samples were

allowed to cool to room temperature under the same N_2 environment to ensure controlled conditions. For electrical characterization, semitransparent Au electrodes (~ 50 nm of thickness) with areas of $95 \times 95 \mu m^2$ spaced by $30 \mu m$ were thermally evaporated through a shadow mask as top contacts. Aluminum with a thickness of ~ 300 nm was used as back contact.

The thickness and the optical constants, refractive index and extinction coefficient, were determined by ellipsometric measurements using a Variable Angle Spectroscopic Ellipsometer J.A. Woollam M—2000U, (J.A. Woollam Co., Lincoln, NE, USA). The measurements were carried out at three angles of incidence in the range of 50 – 70° . The experimental results for the ellipsometric angles Ψ and Δ were fitted in the 400 – 1000 nm range using the Cauchy dispersion model. The surface morphologies of NiO_x layers deposited on Si were characterized using AFM instrument NX10 (Park Systems Co., Suwon, Republic of Korea) Park Systems, Republic of Korea. The AFM was equipped with an anti-acoustic box and an active vibration isolation table to prevent noises and vibrations that can affect the measurements. The measurements were carried out with a PPP-NCHR probe tip (Park Systems Co., Suwon, Republic of Korea) with a force constant $k = 42$ N/m and a resonance frequency of 330 kHz using the non-contact mode. The scanned area was $1 \times 1 \mu m^2$. Electrical characterization was carried out using a Keithley 4200-SCS Semiconductor Characterization System, (Tektroniks Inc., Beaverton, OR, USA). I - V dependencies were measured in the dark and under illumination with red, green, blue and UV light-emitting diodes (LEDs). The LEDs' optical power intensities are given in Table 5. C - V characteristics were measured in the dark at a frequency of 100 kHz using a test signal with an amplitude of 30 mV. The bias sweep delay time and hold time for the I - V and C - V measurements were 0.5 s and 1 s, respectively, while the voltage steps used were 50 or 100 mV.

Table 5. Optical power of the light-emitting diodes used in this study [27].

Color	Photon Wavelength/Energy (nm/eV)	Optical Power Intensity (mW/cm ²)
Red	635/1.95	3.71
Green	530/2.34	1.03
Blue	400/3.10	1.31
UV	365/3.40	0.335

5. Conclusions

Photodetectors with high responsivity in self-powered mode and at a reverse bias of -4 V were fabricated by depositing r.f.-sputtered NiO_x layers on n-Si at RT, 50 °C and 100 °C. The increase of the deposition temperature leads to a decrease of R at $V = 0$ V and $V_r = -4$ V, but at the same time to a smaller dark current at reverse biases. In addition, higher deposition temperature leads to an increase of the diodes' series resistance and of the NiO_x resistivity. The diodes fabricated after RTA annealing show much higher R compared to those with as-deposited layers. A disadvantage of these diodes is the dependence of their dark current and photocurrents on the direction of the bias voltage change. As a result, the annealed diodes may be inappropriate for applications where exact determination of the optical power is required, but because of the very high responsivity, they might be useful as light sensors.

Author Contributions: Conceptualization, N.N., D.M.-A. and R.N.; methodology, D.M.-A., R.N., B.V.-S. and J.L.-M.; software, R.N., E.O.-E. and D.M.-A.; validation, D.M.-A. and R.N.; formal analysis, N.N.; investigation, E.O.-E. and E.O.-U.; resources, B.V.-S., N.N., M.C.-A. and D.M.-A.; data curation, R.N. and E.O.-E.; writing—original draft preparation, R.N., E.O.-E. and D.M.-A.; writing—review and editing, O.P.-L., M.C.-A., J.C.-S., B.V.-S. and N.N.; visualization, N.N., D.M.-A. and R.N.; supervision,

B.V.-S.; project administration, N.N. and M.C.-A. All authors have read and agreed to the published version of the manuscript.

Funding: This research received no external funding

Data Availability Statement: The data presented in this study are available on request from the corresponding author.

Acknowledgments: E. Osuna and E. Osorio, gratefully acknowledges the National Council for Science and Technology (CONACYT), Mexico for a M. Eng. and Ph.D. fellowships. We acknowledge the help of Ivan Cardoza-Navarro and Jorge Salvador-Carlos in sample preparation and analysis.

Conflicts of Interest: The authors declare no conflicts of interest.

References

1. Napari, M.; Huq, T.N.; Hoye, R.L.Z.; MacManus-Driscoll, J.L. Nickel oxide thin films grown by chemical deposition techniques: Potential and challenges in next-generation rigid and flexible device applications. *InfoMat* **2021**, *3*, 536–576. [[CrossRef](#)]
2. Aivalioti, C.; Manidakis, E.G.; Pelekanos, N.T.; Androulidaki, M.; Tsagaraki, K.; Viskadourakis, Z.; Spanakis, E.; Aperathitis, E. Niobium-doped NiO as p-type nanostructured layer for transparent photovoltaics. *Thin Solid Films* **2023**, *778*, 139910. [[CrossRef](#)]
3. Wang, F.; Zhang, W.; Jia, J.; Chen, Y.; Chen, Z.; Wang, Z.; Zhang, L.; Ma, H. Improvement of electrochromic properties of NiO film doped with ZnO prepared by magnetron sputtering. *J. Mater. Sci. Mater. Electron.* **2024**, *35*, 455. [[CrossRef](#)]
4. Li, C.; Choi, P.G.; Kim, K.; Masuda, Y. High performance acetone gas sensor based on ultrathin porous NiO nanosheet. *Sens. Actuators B Chem.* **2022**, *367*, 132143. [[CrossRef](#)]
5. Peng, Y.; Jiang, D.; Zhao, M.; Duan, Y.; Wei, H.; Li, H.; Liang, Q.; Wang, S. High-performance UV-visible photodetectors based on ZnO/perovskite heterostructures. *J. Alloys Compd.* **2023**, *965*, 171372. [[CrossRef](#)]
6. Chen, L.; Wang, Y.; Zhang, J.; Chen, L.; Zhai, J.; Song, J. Inorganic Semiconductor-Based Flexible UV Photodetector Arrays Achieved by Specific Flip-Chip Bonding. *ACS Appl. Mater. Interfaces* **2024**, *16*, 51089–51096. [[CrossRef](#)]
7. Castillo-Saenz, J.R.; Nedev, N.; Valdez-Salas, B.; Bernechea, M.; Martínez-Guerra, E.; Mendivil-Palma, I.; Curiel-Alvarez, M.; Mateos, D.; Perez-Landeros, O. Effect of oxidation temperature on the properties of NiO_x layers for application in optical sensors. *Thin Solid Films* **2021**, *734*, 138849. [[CrossRef](#)]
8. Ahmed, A.A.; Hashim, M.R.; Qahtan, T.F.; Rashid, M. Preparation and characteristics study of self-powered and fast response p-NiO/n-Si heterojunction photodetector. *Ceram. Int.* **2022**, *48*, 20078–20089. [[CrossRef](#)]
9. Wang, J.; Li, Q.; Mi, W.; Wang, D.; Xu, M.; Xiao, L.; Zhang, X.; Luan, C.; Zhao, J. Fast response self-powered solar-blind UV photodetector based on NiO/Ga₂O₃ p-n junction. *Mater. Sci. Semicond. Process.* **2025**, *186*, 109084. [[CrossRef](#)]
10. Hwang, J.-D.; Cheng, Y.-A. Enhancing the Performance of NiO-Based Metal-Semiconductor-Metal Ultraviolet Photodetectors Using a MgO Capping Layer. *IEEE Sens. J.* **2021**, *21*, 27400–27404. [[CrossRef](#)]
11. Caglar, M.; Sever, K.; Aktas, S.; Demiroglu, A. Improving the electrical performance of NiO based photodiode fabricated by sol-gel process with Al doping. *Sens. Actuators A Phys.* **2023**, *350*, 114099. [[CrossRef](#)]
12. Pandit, B.; Parida, B.; Jang, H.-S.; Heo, K. Self-Powered Broadband Photodetector Based on NiO/Si Heterojunction Incorporating Graphene Transparent Conducting Layer. *Nanomaterials* **2024**, *14*, 551. [[CrossRef](#)] [[PubMed](#)]
13. Wilson, R.L.; Macdonald, T.J.; Lin, C.-T.; Xu, S.; Taylor, A.; Knapp, C.E.; Guldin, S.; McLachlan, M.A.; Carmalt, C.J.; Blackman, C.S. Chemical vapour deposition (CVD) of nickel oxide using the novel nickel dialkylaminoalkoxide precursor [Ni(dmamp')₂] (dmamp' = 2-dimethylamino-2-methyl-1-propanolate). *RSC Adv.* **2021**, *11*, 22199–22205. [[CrossRef](#)] [[PubMed](#)]
14. Aydin, E.; Troughton, J.; Bastiani, M.D.; Ugur, E.; Sajjad, M.; Alzahrani, A.; Neophytou, M.; Schwingenschlöggl, U.; Laquai, F.; Baran, D.; et al. Room-Temperature-Sputtered Nanocrystalline Nickel Oxide as Hole Transport Layer for p-i-n Perovskite Solar Cells. *ACS Appl. Energy Mater.* **2018**, *1*, 6227–6233. [[CrossRef](#)]
15. Meng, X.; Gao, X.; Du, Y. Influence of O₂/Ar flow ratio on the structure, optical and electrical properties of DC reactively magnetron-sputtered face-centered cubic NiO films at room temperature. *Phys. Rev. B Condens. Matter* **2020**, *579*, 411877. [[CrossRef](#)]
16. Timoshnev, S.; Kazakin, A.; Shubina, K.; Andreeva, V.; Fedorenko, E.; Koroleva, A.; Zhizhin, E.; Koval, O.; Kurinnaya, A.; Shalin, A.; et al. Annealing Temperature Effect on the Physical Properties of NiO Thin Films Grown by DC Magnetron Sputtering. *Adv. Mater. Interfaces* **2024**, *11*, 2300815. [[CrossRef](#)]
17. Wang, H.; Zhao, Y.; Li, X.; Zhen, Z.; Li, H.; Wang, J.; Tang, M. Effect of Sputtering Temperature on Structure and Optical Properties of NiO Films Fabricated by Magnetron Sputtering. *J. Electron. Mater.* **2017**, *46*, 4052–4056. [[CrossRef](#)]
18. Jamal, M.S.; Shahahmadi, S.A.; Chelvanathan, P.; Alharbi, H.F.; Karim, M.R.; Dar, M.A.; Luqman, M.; Alharthi, N.H.; Al-Harathi, Y.S.; Aminuzzaman, M.; et al. Effects of growth temperature on the photovoltaic properties of RF sputtered undoped NiO thin films. *Results Phys.* **2019**, *14*, 102360. [[CrossRef](#)]

19. Ahmed, A.A.; Hashim, M.R.; Rashid, M. Effect of RF power on structural, morphological and optical properties of NiO thin films. In Proceedings of the AIP Conference, Kelantan, Malaysia, 6 February 2019.
20. Elmassi, S.; Narjis, A.; Nkhaili, L.; Elkissani, E.; Amiri, L.; Drissi, S.; Abali, A.; Bousseta, M.; Outzourhit, A. Effect of annealing on structural, optical and electrical properties of nickel oxide thin films synthesized by the reactive radio frequency sputtering. *Phys. B Condens. Matter* **2022**, *639*, 413980. [[CrossRef](#)]
21. Abdur, R.; Choudhury, S.; Bashar, M.S.; Hossain, M.R.; Quddus, M.S.; Akhtar, U.S.; Shaikh, M.A.A.; Hossain, M. Enhancing perovskite solar cell performance: Investigating the impact of post-annealing on the optoelectrical and structural properties of RF-sputtered NiO films via SCAPS-1D device modeling. *Sol. Energy* **2024**, *271*, 112443. [[CrossRef](#)]
22. Koushik, D.; Jošt, M.; Dučinskas, A.; Burgess, C.; Zardetto, V.; Weijtens, C.; Verheijen, M.A.; Kessels, W.M.M.; Albrecht, S.; Creatore, M. Plasma-assisted atomic layer deposition of nickel oxide as hole transport layer for hybrid perovskite solar cells. *J. Mater. Chem. C* **2019**, *7*, 12532–12543. [[CrossRef](#)]
23. Abzieher, T.; Moghadamzadeh, S.; Schackmar, F.; Eggers, H.; Sutterlütü, F.; Farooq, A.; Kojda, D.; Habicht, K.; Schmager, R.; Mertens, A.; et al. Electronbeam-evaporated nickel oxide hole transport layers for perovskite-based photovoltaics. *Adv. Energy Mater.* **2019**, *9*, 1802995. [[CrossRef](#)]
24. Hasan, M.R.; Xie, T.; Barron, S.C.; Liu, G.; Nguyen, N.V.; Motayed, A.; Rao, M.V.; Debnath, R. Self-powered p-NiO/n-ZnO heterojunction ultraviolet photodetectors fabricated on plastic substrates. *APL Mater.* **2015**, *3*, 10610. [[CrossRef](#)] [[PubMed](#)]
25. Schroder, D.K. *Semiconductor Material and Device Characterization*, 3rd ed.; John Wiley & Sons: Hoboken, NJ, USA, 2006; p. 187.
26. Grilli, M.L.; Aydogan, S.; Yilmaz, M. A study on non-stoichiometric p-NiO_x/n-Si heterojunction diode fabricated by RF sputtering: Determination of diode parameters. *Superlattices Microstruct.* **2016**, *100*, 924–933. [[CrossRef](#)]
27. Mateos-Anzaldo, D.; Nedev, R.; Perez-Landeros, O.; Curiel-Alvarez, M.; Castillo-Saenz, J.; Arias-Leon, A.; Valdez-Salas, B.; Silva-Vidaurre, L.; Martinez-Guerra, E.; Osorio-Urquiza, E.; et al. High-performance broadband photodetectors based on sputtered NiO_x/n-Si heterojunction diodes. *Opt. Mater.* **2023**, *145*, 114422. [[CrossRef](#)]
28. Chen, X.; Ren, F.; Gu, S.; Ye, J. Review of gallium-oxide-based solar-blind ultraviolet photodetectors. *Photonics Res.* **2019**, *7*, 381–415. [[CrossRef](#)]
29. Hammadi, O.A.; Khalaf, M.K.; Kadhim, F.J. Fabrication of UV Photodetector from Nickel Oxide Nanoparticles Deposited on Silicon Substrate by Closed-Field Unbalanced Dual Magnetron Sputtering Techniques. *Opt. Quantum Electron.* **2015**, *47*, 3805–3813. [[CrossRef](#)]
30. Ahmed, A.A.; Hashim, M.R.; Qahtan, T.F.; Rashid, M. Multi—Wavelength Photodetectors Based on Porous Spin-Coated and Compact RF-Sputtered NiO Films Grown over Si Substrate: Effect of Surface Morphology. *Optik* **2022**, *255*, 168694. [[CrossRef](#)]
31. Xu, J.; Cao, R.; Shi, S.; Li, L.; Zhu, K.; Su, Y. Self-Powered Ultraviolet Photodetectors Based on Match like Quasi One-Dimensional N-TiO₂/P-NiO Core-Shell Heterojunction Arrays with NiO Layer Sputtered at Different Power. *J. Alloys Compd.* **2022**, *928*, 167126. [[CrossRef](#)]
32. Enns, Y.; Timoshnev, S.; Kazakin, A.; Shubina, K.; Uvarov, A.; Vorobyev, A.; Nikitina, E.; Mizerov, A.; Andreeva, V.; Fedorenko, E.; et al. Characterization of the P-NiO/N-GaN Heterojunction and Development of Ultraviolet Photodiode. *Mater. Sci. Semicond. Process.* **2024**, *181*, 108624. [[CrossRef](#)]
33. Ma, X.; Tang, L.; Jia, M.; Zhang, Y.; Zuo, W.; Cai, Y.; Li, R.; Yang, L.; Teng, K.S. Ultrahigh Performance UV Photodetector by Inserting an Al₂O₃ Nanolayer in NiO/N-Si. *Adv. Electron. Mater.* **2024**, *10*, 2300909. [[CrossRef](#)]

Disclaimer/Publisher’s Note: The statements, opinions and data contained in all publications are solely those of the individual author(s) and contributor(s) and not of MDPI and/or the editor(s). MDPI and/or the editor(s) disclaim responsibility for any injury to people or property resulting from any ideas, methods, instructions or products referred to in the content.